

Distortion-matched T_1 maps and unbiased T_1 -weighted images as anatomical reference for high-resolution fMRI

Wietske van der Zwaag^{a,*}, Pieter F. Buur^a, Alessio Fracasso^{a,b}, Tessa van Doesum^a, Kâmil Uludağ^c, Maarten J. Versluis^d, José P. Marques^e

^a Spinoza Centre for Neuroimaging, Amsterdam, The Netherlands

^b Institute of Neuroscience and Psychology, University of Glasgow, Glasgow G12 8QB, UK

^c Maastricht University, Maastricht, The Netherlands

^d Philips Healthcare, Eindhoven, The Netherlands

^e Donders Institute for Brain, Cognition and Behaviour, Nijmegen, The Netherlands

ARTICLE INFO

Keywords:

T_1 -weighted EPI
Bias field
Functional MRI
Distortion
Surface definition

ABSTRACT

The increasing availability of ultra-high field scanners has led to a growing number of submillimetre fMRI studies in humans, typically targeting the gray matter at different cortical depths. In most analyses, the definition of surfaces at different cortical depths is based on an anatomical image with different contrast and distortions than the functional images. Here, we introduce a novel sequence providing bias-field corrected T_1 -weighted images and T_1 -maps with distortions that match those of the fMRI data, with an image acquisition time significantly shorter than standard T_1 -weighted anatomical imaging. For ' T_1 -imaging with 2 3D-EPIs', or T_1 23DEPI, 3D-EPI volumes are acquired centred at two inversion times. These 3D-EPIs are segmented into half, quarter or smaller blocks of k-space to allow for optimisation of the inversion times. T_1 -weighted images and T_1 -maps are then generated as for MP2RAGE acquisitions. A range of T_1 23DEPI data acquired at 7 T is shown with resolutions ranging from 0.7 mm to 1.3 mm isotropic voxels. Co-registration quality to the mean EPI of matching fMRI timecourses shows markedly less local deviations compared to co-registration of a standard MP2RAGE to the same echo planar volume. Thus, the T_1 23DEPI T_1 -weighted images and T_1 -maps can be used to provide cortical surfaces with matched distortions to the functional data or else to facilitate co-registration between functional and undistorted anatomical data.

Introduction

The limited anatomical contrast in T_2^* -weighted images means that nearly all fMRI sessions require the acquisition of a separate dataset with sufficient anatomically relevant contrast. Usually, this is a T_1 -weighted gradient echo e.g. Magnetisation Prepared Rapid Gradient Echo or MPRAGE (Mugler and Brookeman, 1990), which provides good gray-white matter contrast in a reasonable scan time. At ultra-high field, (i.e. 7T or higher), the B_1 -inhomogeneities favour the use of B_1 -insensitive strategies (Marques et al., 2010; Mougin et al., 2016; Van de Moortele et al., 2009). For most pulse sequences, these anatomical reference data differ from the functional data in contrast, the amount of susceptibility-induced distortions and, often, in the amount of brain coverage. This complicates the co-registration between these two data types. For example, the use of registration methods that rely on internal

edge information, such as boundary based registration (Greve and Fischl, 2009), assume that the boundaries are at the same location in all images, which is not guaranteed in images with different contrasts and different distortions. However, the impact of these registration imperfections for standard mapping studies is limited, as the functional data often undergoes smoothing in pre-processing and both the functional and anatomical data are transformed and normalised into a standard space.

More and more 7T data is acquired at sub-millimetre resolution to study functional responses from different cortical depths (Huber et al., 2015; Kok et al., 2016; Koopmans et al., 2011; Polimeni et al., 2010) or columns (Yacoub et al., 2007; Zimmermann et al., 2011), to address a new range of neuroscientific questions (Dumoulin et al., 2017). For this type of data, the (even small) local and global differences in distortions become more problematic. Surfaces at different cortical depths are usually defined in the anatomical dataset and subsequently overlaid on the

* Corresponding author. Spinoza Centre for Neuroimaging Meibergdreef 75, 1105 BK Amsterdam, The Netherlands.

E-mail address: w.vanderzwaag@spinozacentre.nl (W. van der Zwaag).

<https://doi.org/10.1016/j.neuroimage.2018.04.026>

Received 19 January 2018; Received in revised form 5 April 2018; Accepted 10 April 2018

Available online 14 April 2018

1053-8119/© 2018 The Authors. Published by Elsevier Inc. This is an open access article under the CC BY-NC-ND license (<http://creativecommons.org/licenses/by-nc-nd/4.0/>).

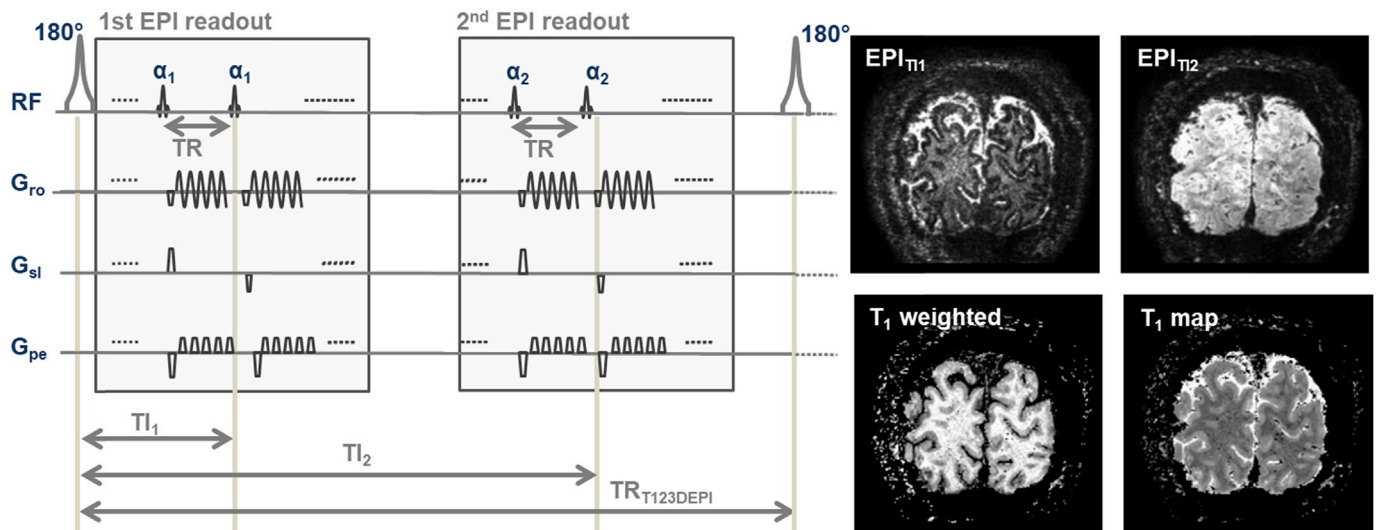


Fig. 1. Sequence diagram. An (adiabatic) inversion pulse is followed by two EPI readout blocks at T_{I1} and T_{I2} . These EPI blocks can contain the sampling of an entire k-space, in which case a full T_1 -weighted images and T_1 map are acquired after $1 \text{ TR}_{T_{I23DEPI}}$. For larger k-spaces it is likely to be necessary to split these acquisitions so that half or a quarter k-space is acquired after each inversion. Data from the two echo planar images (inserts, top) are combined as for the MP2RAGE sequence to generate T_1 -maps and T_1 -weighted images (inserts bottom).

functional data, from which the depth-dependent signals are derived. To optimally benefit from the advantages of 7T, these anatomical data are usually acquired using tailored or carefully selected sequences (Marques and Norris, 2017) and great care is taken to correctly derive the desired surfaces (Kemper et al., 2017). For these data, which are often not averaged over subjects in a standard space but treated individually, spatial accuracy is of paramount importance to obtain functional responses specifically arising from the cortical depth they are assigned to (Polimeni et al., 2017). In practice, it is challenging to achieve an accurate and reliable geometric distortion correction (Hutton et al., 2002; Irfanoglu et al., 2015). Hence, it is advantageous to acquire a reference with anatomical contrast and with identical susceptibility-induced distortions as the functional data. In addition, it is important that such an acquisition is relatively fast as the high-resolution functional sessions already take up large amounts of scantime and re-acquisition of the anatomy in multiple scanning sessions may be necessary.

T_1 -weighted echo planar data or T_1 -maps based on echo planar readouts have been suggested for use as anatomical reference previously, but have so far not been widely used. Most methods suffer from either limited spatial resolution (Gowland and Mansfield, 1993; Wright et al., 2008) or modest brain coverage that can be achieved, for example when preceding an echo volumar readout with an inversion pulse (van der Zwaag et al., 2006), or else from the long acquisition times associated with the combination of multislice acquisitions and inversion pulses (Brammer et al., 1997). This long sampling time can be improved by clever reordering of slices (Kashyap et al., 2017; Renvall et al., 2016) or the use of a 3D-EPI readout, which has been compared to more standard T_1 -weighted anatomical images in lesion detection, but then found to suffer from susceptibility induced distortions (Karantanis et al., 1999). One time-efficient, albeit low-SNR, approach is the use of the, usually discarded, first volume of the EPI train to derive a T_1 -map (Bodurka et al., 2007). T_1 -maps are generally preferable to T_1 -weighted images because they are not sensitive to the bias fields associated with variations of flip-angles (Renvall et al., 2016; Wright et al., 2008). It is worth noting that the majority of the studies mentioned here proposed EPI readouts not just because of the possible time-savings, but especially because of the matching distortions to the functional EPI data (Bodurka et al., 2007; Brammer et al., 1997; Huber et al., 2016b; Kashyap et al., 2017; Renvall et al., 2016).

In this study, to match the distortions between functional and structural scans, we modified a 3D-EPI sequence, used in our functional

studies, to generate T_1 -weighted echo planar images with an approach similar to that used to obtain T_1 -weighted MP2RAGE images. We term this approach “ T_1 -imaging with 2 3D-EPIs” or T_1 23DEPI. Here, the two GRE readout blocks (encompassing all phase encoding steps along one dimension) of the MP2RAGE sequence were replaced with two 3D-EPI blocks as shown in Fig. 1. Following the inversion pulse, several segments of a 3D EPI sequence are acquired, with the k-space centre plane being acquired at time T_{I1} , resulting in an heavily T_1 -weighted image. At a later time, an identical EPI train is acquired centred at T_{I2} , generating an image with much less T_1 -weighting. Examples of the acquired images are shown on the right of Fig. 1. The image acquired at T_{I1} has T_1 contrast, but also a strong bias field (note the lower image intensities in the lower right) and T_2^* contrast. The image acquired at T_{I2} has the same bias field and T_2^* contrast as $EPI_{T_{I1}}$ (note again the lower image intensities in the lower right), but not the same T_1 weighting. In the MP2RAGE sequence the complex GRE images are combined following: $S_{MP2RAGE} = (GRE_{T_{I1}} * GRE_{T_{I2}}) / (GRE_{T_{I1}}^2 + GRE_{T_{I2}}^2)$. For the T_1 23DEPI the GRE's are simply replaced with the complex data of the echo planar images: $S_{T_123DEPI} = (EPI_{T_{I1}} * EPI_{T_{I2}}) / (EPI_{T_{I1}}^2 + EPI_{T_{I2}}^2)$. Same as for the MP2RAGE anatomicals, this combination approach removes the T_2^* contrast associated with the EPI readout. Thus, the combination of the two EPI blocks yields bias-field corrected images with homogeneous contrast throughout the covered area, as also obtained with the MP2RAGE sequence. In addition, proton density and receive B_1 sensitivities are also cancelled by the image combination, allowing generation of a T_1 -estimation map via a lookup table (Marques et al., 2010). As the EPI readout duration is equal to that of the functional data, the obtained T_1 estimation maps and bias-field corrected T_{1w} images have distortions matched to those of the functional data. Besides the susceptibility induced distortions, another difference between the T_1 23DEPI and the MP2RAGE sequences is the much reduced acquisition time in the T_1 23DEPI. Following a single inversion pulse, a much larger k-space section is acquired for the T_1 23DEPI than for the MP2RAGE, drastically shortening the time to fill k-space. In the extreme case, if all of k-space can be acquired within a single block, a T_1 -weighted image and T_1 -map can be acquired in a matter of seconds (Huber et al., 2016a, 2016b), namely the time between two inversion pulses, $TR_{T_{I23DEPI}}$.

As acquisition times for a single volume can be relatively long in sub-millimeter fMRI (Batson et al., 2015; Petridou et al., 2013), it may be necessary to split the 3D-EPI volume into several ‘blocks’ containing multiple EPI readouts to allow for an optimal inversion time to be chosen

Table 1
Imaging parameters for the T₁23DEPI data acquired in Experiments 1, 2 and 3.

Name	TR _{T123DEPI}	TI ₁ /TI ₂	α_1/α_2	TR _{EPI}	Averages	FOV	Resolution	T _{acq}	Notes
Experiment 1, 2 blocks	10s	1200/ 3800 ms	14/ 10	57 ms	4	120* 131* 24 mm	0.7* 0.7* 0.7 mm	80s	34 readouts per block
Experiment 1, 4 blocks	8.25s	1000/ 2700 ms	20/ 16	57 ms	4	120* 131* 24 mm	0.7* 0.7* 0.7 mm	132s	18 readouts per block
Experiment 2, 0.8 mm slab	8.25s	1000/ 3200 ms	19/ 16	54 ms	4	150* 169* 24	0.8* 0.8* 0.8	132s	19 readouts per block; Motor task fMRI
Experiment 2, 1 mm whole-brain	8.5 s	1000/ 3200 ms	15/ 13	44 ms	2	200* 212* 120	1.0* 1.0* 1.0 mm	170s	31 readouts per block; 10 blocks; also 10 vol EPI without task
Experiment 2, 1 mm slab	8.00 s	1000/ 3200 ms	19/ 16	48 ms	4	200* 212* 30 mm	1.0* 1.0* 1.0 mm	128s	19 readouts per block; 4 blocks Including reversed readout for distortion correction
Experiment 2, 1.3 mm slab	8.75 s	1000/ 3600 ms	19/ 14	44 ms	4	202* 202* 40	1.3* 1.3* 1.3 mm	140s	18 readouts per block; 4 blocks; Motor task fMRI
Experiment 3, 0.8 mm wholebrain long block	8.25 s	1000/ 3300	19/ 15	53 ms	2	170* 189* 120	0.8* 0.8* 0.8 mm	198s	20 readouts per block; 12 blocks; checkerboard fMRI. Repeated with N = 3
Experiment 3, 0.8 mm wholebrain short block	8.25 s	1000/ 3300	19/ 15	53 ms	2	170* 189* 120	0.8* 0.8* 0.8 mm	561s	6 readouts per block; 34 blocks;

for the 3D-EPI block acquired at TI₁. This segmentation means that, for practically any functional EPI protocol, a T₁-map and T₁-weighted dataset with matching distortions can be acquired.

Methods

A total of 25 healthy volunteers were scanned at 7T (Philips, Netherlands) with a 32-channel receive and 2-channel transmit volume coil (Nova Medical, USA) using different acquisition protocols specified below, some as part of another study. All volunteers provided written informed consent prior to participating in the session. The protocol was approved by the local ethics committee.

All acquisition protocols for MP2RAGE and T₁23DEPI were generated using the Multiple Instantaneously Switchable Scans, MISS, functionality on the Philips platform. Bloch simulations as in (Marques et al., 2010) were used to derive optimal inversion times, TR_{volume} and flip angles for both MP2RAGE and T₁23DEPI protocols.

In Experiment 1, the effect of changing the length of the EPI readout block in the T₁23DEPI was investigated. Two protocols were compared in four volunteers: T₁23DEPI protocols with 3D-EPI readouts split into either 2 or 4 k-space sections (blocks) were separately optimised. A higher (0.7 mm isotropic) 3D-EPI protocol previously used for sub-millimetre fMRI acquisitions (Petridou et al., 2013) was adapted to acquire the T₁23DEPI data. Parameters of this functional 3D-EPI protocol were: FOV 120 × 131 × 24 mm³, matrix size 172 × 188 × 34, TR/TE = 57 ms/28 ms, EPI factor = 27 (i.e. 2 readouts per k-space plane), SENSE undersampling factor 3.5 (LR) * 1.3 (AP), slice oversampling factor 1.28, 68 EPI readouts (segments) per volume, volume acquisition time 3.9 s. No fat saturation was used. Specific parameters for the T₁23DEPI protocols are given in Table 1. The minimum inversion time of the first readout (TI₁) in the 2-block protocol was limited by the length of the readout block. For the 2-block protocol this readout block length was 1.94s, for the 4-block protocol it was 1.03s.

MP2RAGE data were acquired for all subjects as an anatomical reference, with the following parameters: voxel size 0.64 mm isotropic, FOV 220 × 220 × 164 mm³, TR_{MP2RAGE}/TE/TR_{FLASH} = 5.5 s/2.3 ms/6.2 ms, TI₁/TI₂ = 800 ms/2700 ms, α_1/α_2 = 7/5, t_{acq} 11 min. The readout block length of the MP2RAGE was 985 ms, comparable to that of the 4-block protocol described above. For both the MP2RAGE and all T₁23DEPI sequences a non-selective adiabatic inversion pulse (hyperbolic secant) was used.

For two out of these four volunteers, a 4 min functional run using a flashing checkerboard stimulus (Jorge et al., 2015) with 10 s stimulus alternating with 20 s baseline was also acquired using the 0.7 mm 3D-EPI protocol.

In Experiment 2, a range of high-resolution fMRI protocols were

acquired with matching T₁23DEPI data. Details of the different T₁23DEPI protocols are given in Table 1. For all volunteers a 0.64 mm MP2RAGE with parameters as given above was also acquired.

- For two volunteers, a sagittal 0.8 mm T₁23DEPI slab was acquired in 2 min 12 s along with functional data acquired during execution of a simple block design motor-task with 15 s hand movement alternated with 15 s rest with a total functional run duration of 8 min. These data were part of the pilot acquisitions for another study. 3D-EPI parameters were: TE = 28 ms, EPI factor = 27, SENSE undersampling factor 4 (AP), slice oversampling volume 1.28, volume acquisition time 4.1s.
- For two volunteers, a whole-brain 1 mm isotropic slab was acquired in 2.5 min as well as 10 volumes of matching whole-brain EPI data. 3D-EPI parameters were: TE = 21 ms, EPI factor = 27, SENSE undersampling factor 4 (AP), slice oversampling factor 1.28, volume acquisition time 15s. The 1 mm isotropic whole-brain T₁23DEPI were automatically segmented using the standard segmentation pipeline from SPM12 and the automatic pipeline from Freesurfer.
- For 12 volunteers, as part of another study, a 1 mm isotropic oblique coronal slab T₁23DEPI covering the cerebellum, midbrain and part of the frontal cortex was acquired. The temporal mean of a matching functional run was used to demonstrate co-registration quality for an example subject. For both the functional run and the T₁23DEPI data, five separate volumes were acquired with opposing phase-encoding direction (LR rather than RL) to allow distortion correction using FSL's TOPUP (Andersson et al., 2003). From these pairs of images, the susceptibility-induced off-resonance field was estimated and both pairs of images were combined into a single corrected one. 3D-EPI parameters were: TE = 26 ms, EPI factor = 27, SENSE undersampling factor 4 (LR), slice oversampling volume 1.28, volume acquisition time 3.6s. For these data acquisitions, a dielectric pad was used to improve B₁-homogeneity over the cerebellum (Teeuwisse et al., 2012).
- For a further 4 volunteers, a 1.3 mm isotropic coronal oblique slab covering again the cerebellum, midbrain and part of the frontal cortex was acquired. A simple block paradigm motor task alternating 15 s of bilateral finger tapping with 15 s rest was used to elicit functional responses in a 7 min EPI acquisition. 3D-EPI parameters were: TE = 26 ms, EPI factor = 27, SENSE undersampling factor 3 (LR), slice oversampling volume 1.1, volume acquisition time 3.0s.

In Experiment 3, the effects of block length were further tested and BOLD measures were extracted as a function of cortical depth. Two T₁23DEPI datasets were acquired along with an MP2RAGE anatomical and a 5-min functional acquisition using a checkerboard stimulus. The checkerboard was alternating at 8 Hz black and white on a gray

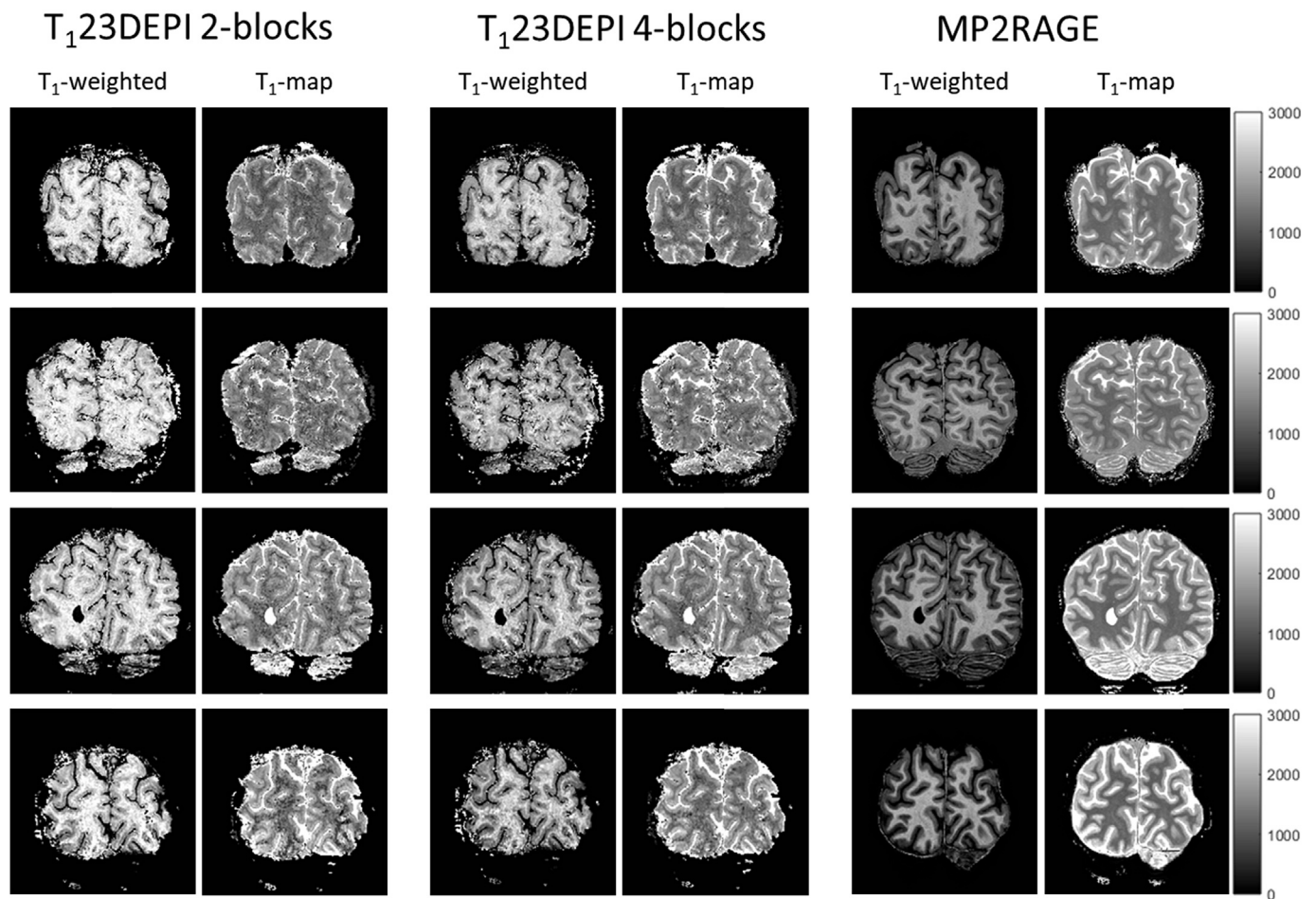


Fig. 2. Example slices from the 0.7 mm isotropic T_1 maps and T_1 -weighted T_1 23DEPI images and comparable slices from the 0.7 mm³ MP2RAGE. All data were skull-stripped and the same intensity range was used for all. Voxels within the brain masks were used to generate the histograms. Note the homogeneous contrast throughout the slices. 2-block data have slightly lower T_1 contrast due to the longer TI_1 , but 4-block T_{1w} - T_1 23DEPI images have near-identical contrast to the MP2RAGE standard. All T_1 maps are of similar contrast. The same gray scale was used for all T_1 maps.

background, 10 s ON, 20 s OFF, for 10 cycles (Jorge et al., 2015). 3D-EPI parameters were: TE = 25.5 ms, EPI factor = 27, SENSE undersampling factor 4 (LR), slice oversampling volume 1.1, volume acquisition time 3.9s. The slab thickness for this functional dataset was not matched to that of the T_1 23DEPI, being only 27 mm in the HF direction (34 slices) while the T_1 23DEPI covered the entire brain. As the EPI factor, in-plane FOV, bandwidth, slice orientation and shim-settings remained the same, all distortions were equal between fMRI and T_1 23DEPI. Two T_1 23DEPI's were acquired with a different block length, but otherwise equal acquisition parameters. Details of the different T_1 23DEPI protocols are given in Table 1. The long block length T_1 23DEPI was repeated three more times to examine the effect of increased SNR on the image intensity distribution.

Data analysis

The amount of T_1 -induced blurring across the slice direction was simulated for the three acquisition protocols in Experiment 1 (MP2RAGE, 2-block and 4-block T_1 23DEPI) in Matlab. An artificial image was made containing a square of 3×3 gray matter voxels ($T_1 = 1.85$ s) in a white matter ($T_1 = 1.15$ s) or CSF ($T_1 = 4$ s) background of 36×36 voxels, in order to be able to simulate the encoding used in Experiment 1. The signal in each compartment at each excitation during the acquisition of the first and second inversion readouts was computed using Block Equations. All these images (2 inversions times number of phase encoding steps per readout block) were Fourier transformed. Synthetic k-

space data was created where each k-space encoding line was obtained from the k-space associated with its actual inversion time. Finally these were inverse Fourier Transformed and combined using the MP2RAGE image combination. The amount of blurring was visualised by comparing the readout direction profile with the slice-direction profile.

Both the MP2RAGE and T_1 23DEPI first and second inversion images were exported and subsequently combined in Matlab (<https://github.com/JosePMarques/MP2RAGE-related-scripts/>). Because of the transmit-coil sensitivity map used in the SENSE reconstruction, the combined phase images do not contain phase singularities and the combination can be done post-coil combination. In the MP2RAGE combination, an inversion efficiency of 0.96 was assumed.

All EPI and MP2RAGE data were co-registered to their matching T_1 23DEPI T_1 -weighted images using the six degrees of freedom rigid body co-registration of SPM12 (www.fil.ion.ucl.ac.uk/spm/software/spm12/) to allow comparisons of local distortions. MP2RAGE data were brain extracted prior to co-registration by combining the gray and white matter masks from the SPM segmentation. These masks were also used to define the ROI's for histograms of image intensity and T_1 -values of the data in Experiment 1 and 3.

All functional data was analysed using SPM, with minimal pre-processing (realignment and smoothing with a FWHM of the voxel size) and a GLM modelling the stimuli as a boxcar convolved with the canonical HRF and including the motion parameters as regressors of no interest. Functional data from Experiment 3 was not smoothed. Figures were generated using Matlab (Mathworks Inc), including the

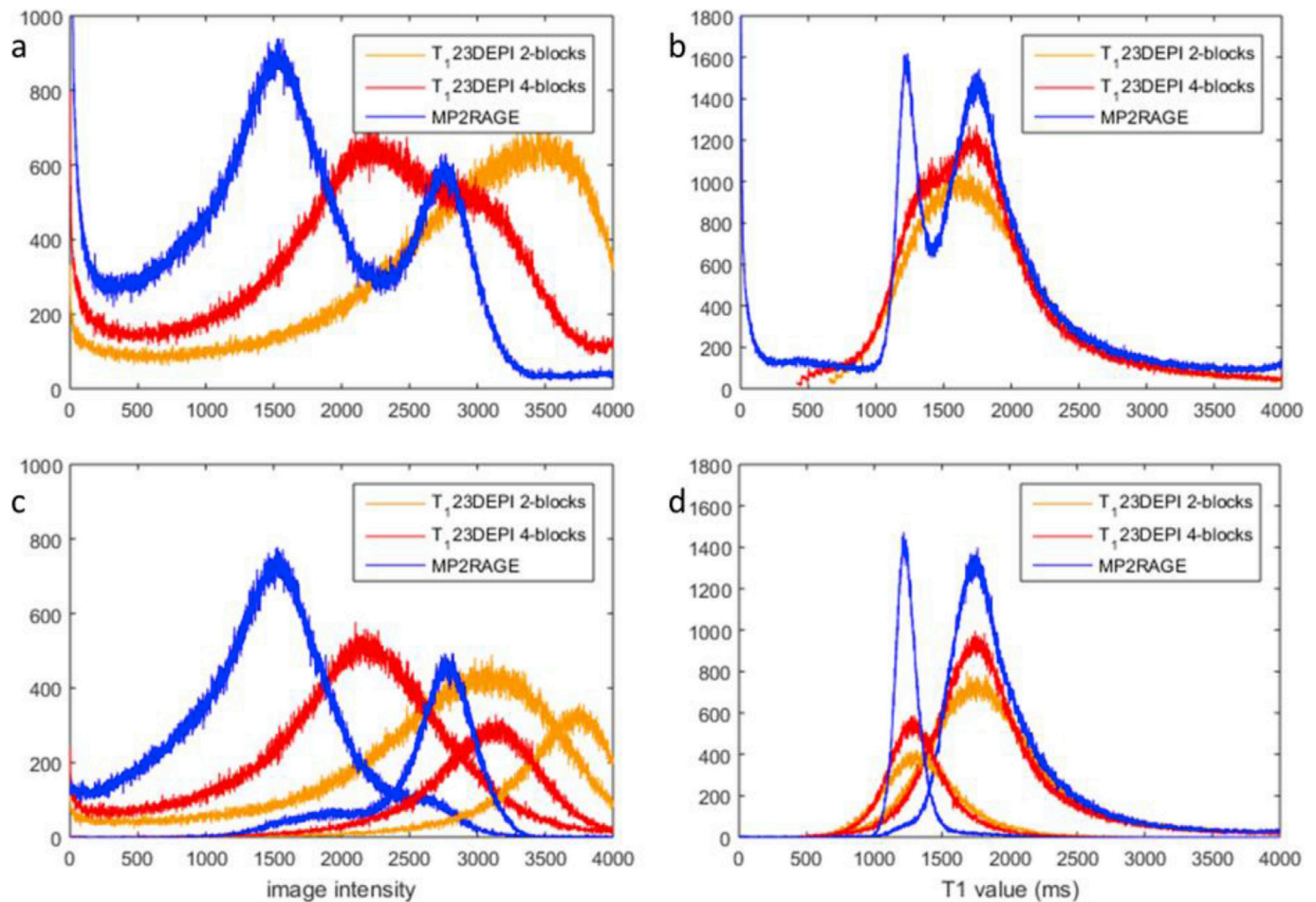


Fig. 3. a) Histograms of image intensities in the 0.7 mm isotropic T_1 -weighted T_1 23DEPI images and co-registered MP2RAGE. b) Histograms of T_1 maps generated from the 0.7 mm isotropic T_1 -weighted T_1 23DEPI images and co-registered MP2RAGE. c) histograms of image intensities from voxels within the gray (lower values) and white (higher values) matter masks obtained from the SPM segmentation. d) histograms of T_1 values from voxels within the gray (centred around ~ 1800 ms) and white (centred around ~ 1100 ms) matter masks. All panels show data grouped over all four datasets shown in Fig. 2. Note that quantitative T_1 values in panels b and d are constant between acquisition types although peak widths depend on the image acquisition type.

image intensity contours used to highlight the gray-white matter and gray matter - CSF boundaries.

The whole-brain T_1 23DEPI T_1 -weighted images, those of experiments 2b and 3, were automatically segmented using SPM and used as input for the standard freesurfer pipeline for cortical surface generation. The unsmoothed functional data acquired in Experiment 3 was projected onto the cortical surfaces generated from the T_1 23DEPI at nine equi-distantly spaced cortical depths using freesurfer's `mri_vol2surf` routine.

Data from Experiments 1 and 3 is freely available online (Van Der Zwaag et al., 2018).

Results

Bloch simulations predicted similar transmit B_1 -sensitivity for the MP2RAGE protocol used here and the T_1 23DEPI protocols of Experiment 1 and 2b (Supplementary Figure 1). The T_1 -induced blurring due to signal evolution during the readout (Supplementary Figure 2a) was negligible for the gray/white matter border in the MP2RAGE and simulated T_1 23DEPI protocols (Supplementary Figure 2b). The gray matter/CSF border showed more blurring particularly for the 2-block protocol of Experiment 1, due to its almost 2-s long readout (Supplementary Figure 2c).

The T_1 23DEPI data acquired in Experiment 1 were compared to the MP2RAGE data in terms of contrast in both the T_1 -weighted images and the T_1 -maps (Fig. 2). As expected from the simulations, contrast in the T_1 -

weighted images differed significantly between the MP2RAGE, T_1 23DEPI 2-block and 4-block data. Most noticeably, the gray-white matter contrast was considerably lower in the 2-block T_1 23DEPI data. On the other hand, T_1 values in the T_1 -maps were remarkably similar across acquisitions. This is confirmed by the histograms of the image intensities presented in Fig. 3: while there are large shifts between T_1 -weighted image intensities in Fig. 3a and c, the T_1 -value histograms in Fig. 3b and d are centred around the same T_1 values for each tissue type. The gray and white matter peaks in the histograms are well separated in the blue MP2RAGE curves in Fig. 3, less so in the red 4-block histograms and nearly merged in the orange histogram of the 2-block data. The increased width of the distribution in the T_1 23DEPI is especially noticeable when looking at the separately plotted distribution for the white and gray matter masks in Fig. 3c and d.

The result of co-registration between the MP2RAGE, T_1 23DEPI and mean EPI volume of the 0.7 mm data is shown in Fig. 4. For reference, the contours of the MP2RAGE data, which was scaled from 0 to 4095, at values 1000 (mid-green) and 2000 (orange) are shown overlaid on the T_1 23DEPI and mean EPI volumes. Although the overall co-registration appears successful, at several locations a mis-match between the MP2RAGE contours and the EPI data exists. Blue arrows in the middle panels indicate troublesome areas in the gray matter surface (light and mid-blue) and the white-gray matter boundary (dark blue). The activation overlaid on the anatomy is mainly located in the gray matter strip, but is also visibly misplaced at some locations. The most notable shift is

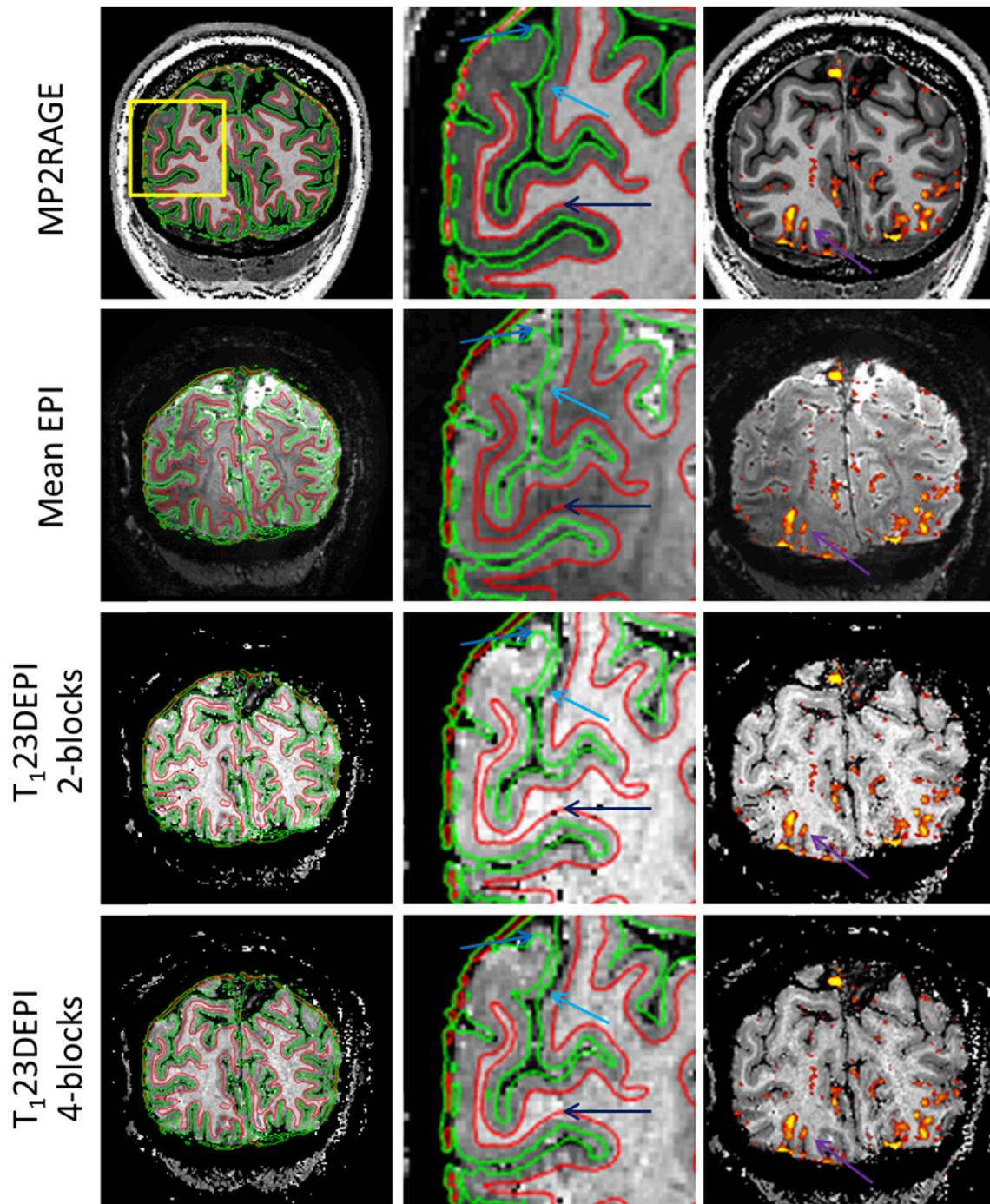


Fig. 4. SPM co-registration results for T_{1w} -images from an MP2RAGE and two $T_{123DEPI}$ acquisitions to a mean EPI volume ($n = 50$). Orange and mid-green contours drawn from the MP2RAGE data (Matlab contour at value 1000 and 2000) correspond roughly to the white/gray matter boundary and gray matter/CSF boundary. Middle row panels display the area marked with a yellow box (top left panel). Blue arrows indicate regions where the MP2RAGE boundaries do not match the anatomical structure seen in the mean EPI. The rightmost panels show the same slices but with the activation map of a visual task overlaid. The purple arrow indicates a region where activation is seemingly on the left bank of the sulcus in the MP2RAGE, yet more equally spread over both banks in the EPI images and both $T_{123DEPI}$'s.

indicated with a purple arrow in the rightmost panels of Fig. 4. While the activation is spread equally over both banks of the sulcus in the mean EPI volume and $T_{123DEPI}$'s, when overlaid on the MP2RAGE it appears more on the leftmost bank of the sulcus. Note here again the improved contrast of the 4-block $T_{123DEPI}$ compared to the 2-block $T_{123DEPI}$.

In Experiment 2, a range of protocols and resolutions were tested in the $T_{123DEPI}$. The first, a 0.8 mm isotropic acquisition with sagittal slice orientation, shows more distortions than the 0.7 mm protocol in Experiment 1 because of the larger portion of brain included in the FOV and the

larger voxel sizes. Co-registration errors are therefore much more pronounced between the distortion-free MP2RAGE and mean EPI, especially anterior and posterior to the central brain portion (Fig. 5, white inset and middle panels). Note that in Fig. 5, all red and green contours are now taken from the $T_{123DEPI}$ image, again at values 1000 (green) and 2000 (red) with the image scaled from 0 to 4095. Significantly active voxels associated with the motor task fall within the gray matter strip both on the $T_{123DEPI}$ and in the MP2RAGE (yellow insets, right panels) because of the central position of the central sulcus and, hence, locally reduced

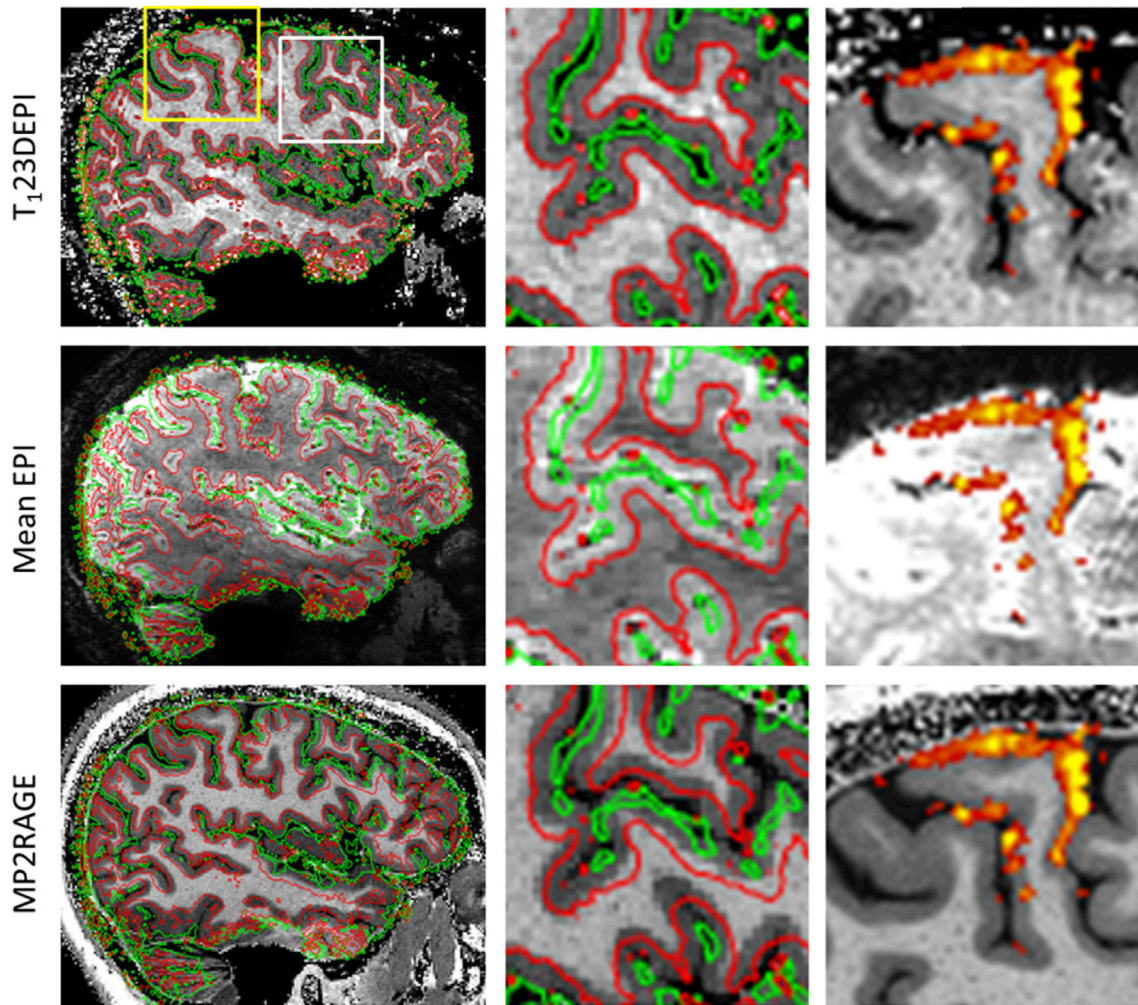


Fig. 5. Image quality and co-registration results for the 0.8 mm sagittal protocol. The mean EPI and MP2RAGE were co-registered to the T₁23DEPI. Red and green contours indicate the white/gray matter boundary and gray matter/CSF boundaries; note that these are in this figure, and in the subsequent figures, drawn from the T₁23DEPI data. The middle column inserts show the area marked in the white box (top left panel). Alignment errors are clearly visible in the MP2RAGE panel (bottom row, middle). The right column inserts show the area marked in yellow (top left panel), which includes the primary motor cortex which was activated by the finger movement task.

distortion.

The T₁23DEPI data acquired with protocol b) of Experiment 2, matched to a 1 mm isotropic whole-brain EPI, can be used in automated segmentation routines such as that of SPM. An example slice from the gray and white matter segment of the result of such a segmentation is shown in the rightmost panel of Fig. 6. The contours in Fig. 6 are drawn from the same segments. The segmentation-boundary follows the gray matter-white matter boundary in the mean EPI faithfully, while small deviations to the MP2RAGE gray-white matter boundary can be observed in the bottom row panels. These deviations signify differences between the MP2RAGE and EPI-based data, and indicate that EPI-based surfaces would be more appropriate for this fMRI protocol than MP2RAGE-based surfaces.

The 1 mm slab images (Table 1) that were also acquired with reversed phase-encoding direction were distortion corrected prior to the co-registration steps. For the example subject, both EPI to T₁23DEPI and MP2RAGE to T₁23DEPI co-registration steps were successful, with good alignment of the internal structures (Fig. 7). The T₁23DEPI contours closely match the anatomic structures in both the MP2RAGE and mean EPI throughout. To investigate the utility of the T₁23DEPI as intermediate in the co-registration pipeline, co-registration of the fMRI data to the MP2RAGE was undertaken with and without the T₁23DEPI step for all twelve volunteers and visually inspected. For three out of twelve

volunteers, the co-registration was improved when the T₁23DEPI was included, for the other nine no differences were found.

The results for an example subject of the 1.3 mm run with motor task are shown in Fig. 8. The motor task yields activation in the entire motor network, including the left and right cerebellar lobule V, left and right primary motor areas and the supplementary motor area (SMA) (Fig. 8, right panels). Overlaid on the T₁-weighted images from the T₁23DEPI and MP2RAGE the activation is seen to be limited to the gray matter strip, even in the finely structured gray matter of the cerebellum. The small clusters in the cerebellum necessitate high accuracy of segmentation and co-registration to correctly identify the folia in which the clusters of activated voxels are found. The T₁23DEPI contours are generally well-aligned with the structures in the mean EPI and MP2RAGE, though some white matter regions in the MP2RAGE are misaligned with the contours because of the susceptibility-induced distortions in the echo planar images (Fig. 8, blue arrows).

The distribution of image intensities in the longer and shorter readout T₁23DEPI data acquired in Experiment 3 were compared to the MP2RAGE image intensity and T₁ distributions to test the effect of block length (or T₁-induced blurring) and increased averaging (or SNR) on the width of the histogram peaks. Image intensities differed between the four protocols (Fig. 9A and C). The peaks of the N = 3 acquisition were somewhat narrower than the long and short readout blocks, which were

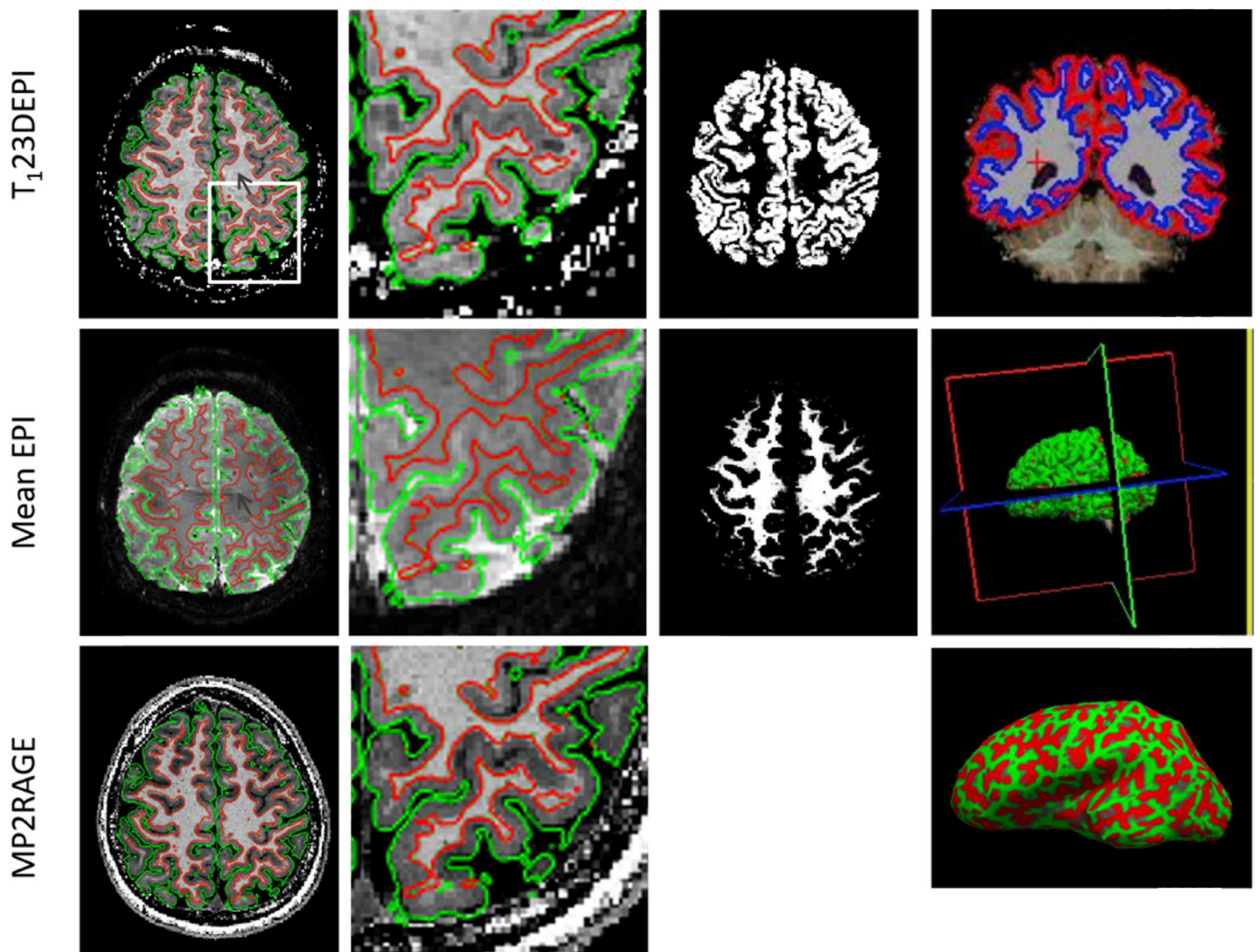


Fig. 6. Image quality and co-registration results for the 1 mm whole-brain protocol. The mean EPI and MP2RAGE were co-registered to the T₁23DEPI. The red and green contours on these example slices indicate the outline of the white matter and gray matter boundaries from the automated segmentation of the T₁23DEPI. The gray arrow in the T₁23DEPI and mean EPI panels indicates a region affected by a SENSE artefact, visible as a near-horizontal line of higher (in the T₁23DEPI) or lower (mean EPI) intensity traversing the white matter. The second column inserts show the area marked in the white box (top left panel). The third column shows for the same slice the gray and white matter masks of the automated SPM segmentation. The last column shows the result of the freesurfer automatic pipeline: the brain extracted image with the pial and white surfaces overlaid, the cortical surface in 3D and finally the inflated cortical surface of the left hemisphere with the curvature measures overlaid in red/green.

similar in height. Note that the number of pulses in the readout train influences the intensity distribution in the MP2RAGE images, and hence, in Fig. 9A and C, the peaks in the short readout block protocol in red are in a different position to those in the long and $N = 3$ acquisitions. The lookup-table for the T₁-map takes this into account, yielding correct, overlapping, T₁-value peaks in Fig. 9B and D. Both 9-min scans, with either more averaging or shorter readouts, led to slightly sharper peaks in the T₁-value distributions (Fig. 9B and D), but the MP2RAGE distribution had the narrowest peaks, especially for the white matter compartment (Fig. 9D).

The 3-min T₁23DEPI data was successfully put through the fully automatic freesurfer pipeline. Fig. 10 shows the BOLD responses to the 5-min visual task overlaid on the mid-gray matter surfaces of the T₁23DEPI and MP2RAGE. The white matter surface (yellow) and pial surface (purple) from the freesurfer segmentation are shown overlaid on the T₁23DEPI along with intermediate cortical depths (25%, 50% and 75%) overlaid on the T₁23EPI data and its segmentation mask. Fig. 10D shows an enlarged version of the white box in Fig. 10C. The average t-values as a function of relative cortical depth are shown for both surfaces defined on both the T₁23DEPI and MP2RAGE data. For both ROIs and both

anatomical scans the BOLD signal increased towards the cortical surface. When mapped onto the T₁23DEPI surfaces the responses in the right hemisphere ROI were similar to when mapped onto the MP2RAGE. For the left hemisphere ROI, the BOLD increase toward the cortical surface was less steep for the MP2RAGE-based surfaces, most likely due to the imperfections in the coregistration (6-parameter rigid body).

A more quantitative comparison in of the MP2RAGE and T₁23DEPI-derived surfaces is presented in Fig. 11. The image intensity values from the mean of the functional run from Experiment 3 were extracted for three Freesurfer-generated ROIs in the occipital lobe, one on the posterior brain surface (ROI1), one along the calcarine sulcus (ROI2) and one more anterior (ROI3). For each ROI, values were extracted from (1) the overlapping region between MP2RAGE and T₁23DEPI segmentation results (Fig. 11, black histograms), (2) the voxels exclusively included in the T₁23DEPI-derived segmentation (Fig. 11, red histograms) and (3) voxels exclusively included in the MP2RAGE-derived segmentation (Fig. 11, blue histograms). The peak of the T₁23DEPI-only histogram (red) was closer to the maximum of the joint ROI histogram (black) for both ROI2 and ROI3, indicating that the image intensity in the T₁23EPI voxels was more similar to the joint region than that of the MP2RAGE-

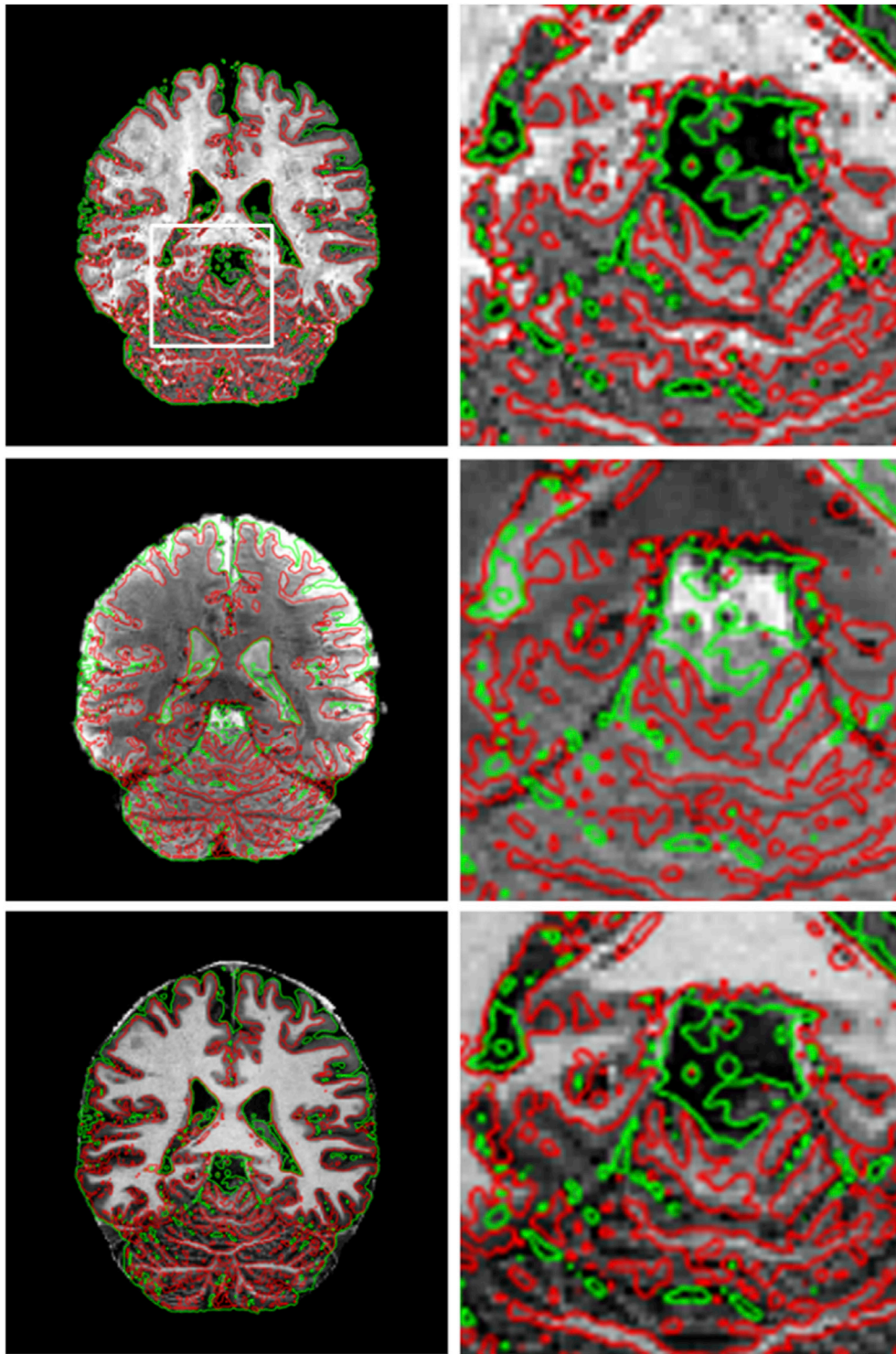


Fig. 7. Image quality and co-registration results for the 1 mm slab protocol. The mean EPI and MP2RAGE were co-registered to the T_1 23DEPI following TOPUP distortion correction of both the functional EPI's and the T_1 23DEPI. Red and green contours indicate the white/gray matter boundary and gray matter/CSF boundary in the T_1 23DEPI. The right column images show an enlargement of the central area outlined in white in the top left panel. Although for this example subject alignment around the cerebellum was good, in general the alignment of the mean EPI of this protocol to the MP2RAGE was more reliable when the T_1 23DEPI volume was used as an intermediate step.

only voxels. More importantly, some of the histograms in ROI1 and ROI2 have a shoulder with low-intensity voxels. These voxels lie outside the brain, and are included in the ROI where the pial surface of the ROI deviates from the pial surface in the EPI. In the MP2RAGE-only histograms, these shoulders of low-intensity voxels are much more pronounced. The difference is especially large in ROI1, the most posterior ROI, where small distortions immediately lead to the inclusion of non-brain voxels in the ROI. This quantitative comparison, similar to the one presented in [Kashyap et al. \(2017\)](#), shows that the T_1 23DEPI-derived segmentation more faithfully follows the cortical gray matter in the

functional EPI data.

Discussion

Here we presented an acquisition strategy for T_1 -imaging with 2 3D-EPIs, T_1 23DEPI, with which bias-field corrected T_1 -weighted data and T_1 -maps are obtained with the same distortions as in functional echo planar images, in a scan acquisition time of only a few minutes. The availability of T_1 -weighted data with matching distortions to the functional data is especially important for those studies where fine anatomical ROIs or

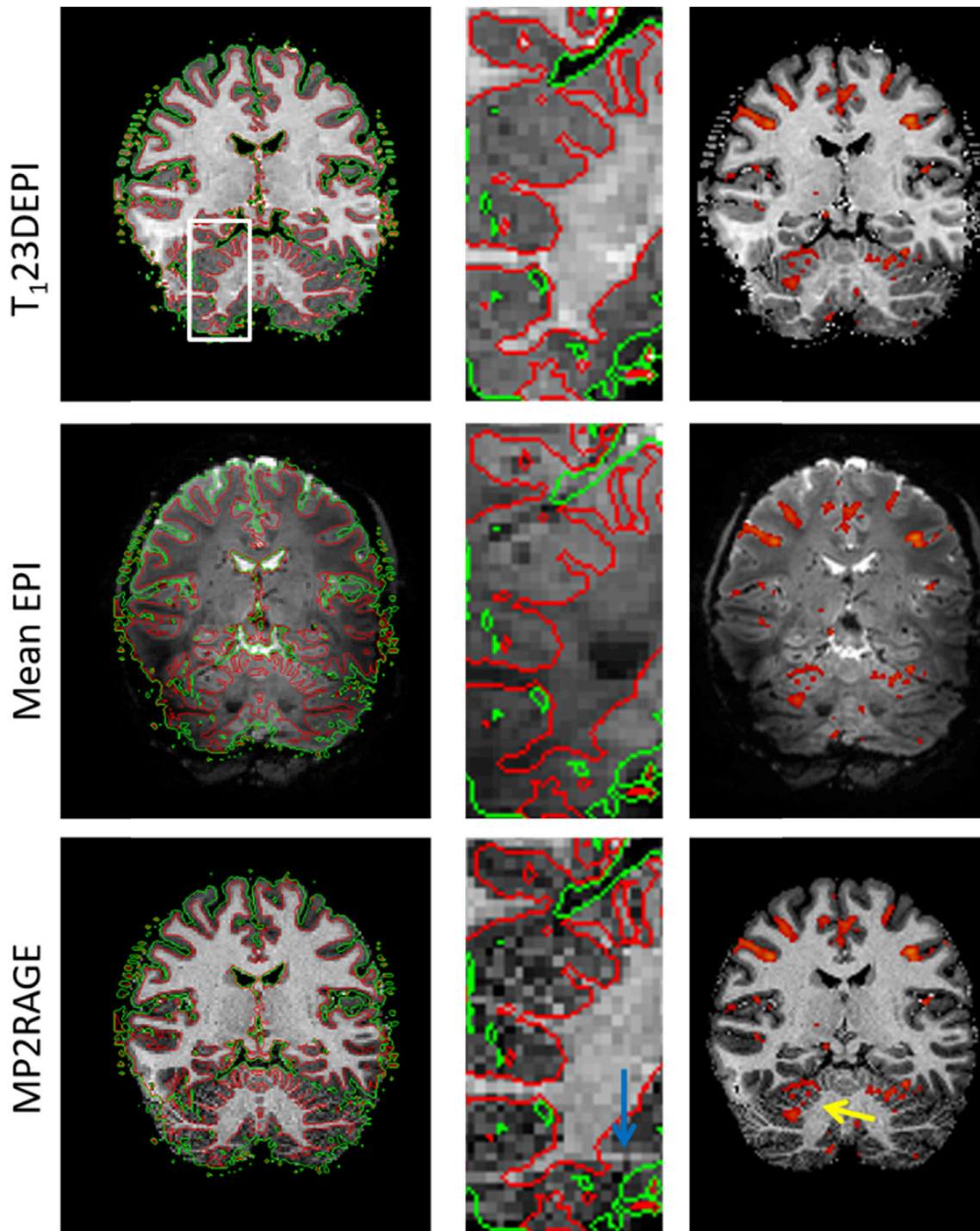


Fig. 8. Image quality, co-registration result and activation map for the 1.3 mm para-coronal slab. Top row: T₁23DEPI data with, in the left panel, contours indicating the gray-white matter boundary (red) and gray matter surface (green) in a coronal oblique slice passing through the cerebellum and crossing the central sulcus. Middle panels show an enlarged region in the cerebellum. The zoomed-in area is outlined in white in the top left panel. The activation map from a hand movement task is overlaid on the same slices in the right panels. The slice traverses the supplementary motor area (midline, top), primary motor cortex (bilateral) and cerebellar lobule V, all showing clusters of significantly active voxels. Middle row: matching slice from the mean EPI volume of the fMRI timecourse with the T₁23DEPI contours (left and middle) and activation map (right) overlaid. Bottom row: matching MP2RAGE slice with the T₁23DEPI contours (left and middle) and activation map (right) overlaid. The blue arrow indicates a region of cerebellar white matter which is not corresponding to white matter in the EPIs due to the distortions therein. The yellow arrow in the right panel indicates small clusters of activation falling within the cerebellar cortical gray matter for which very precise segmentation and co-registration are necessary.

layers are currently obtained from an undistorted anatomical sequence to be used with distorted functional data. Even in functional data with very minor distortions, these will generally be relevant on the millimetre scale. Hence, we expect these T₁23DEPI to be useful for fMRI studies

targeting cortical laminae and/or cortical columns.

These T₁-weighted images and T₁-maps can be used in various ways:

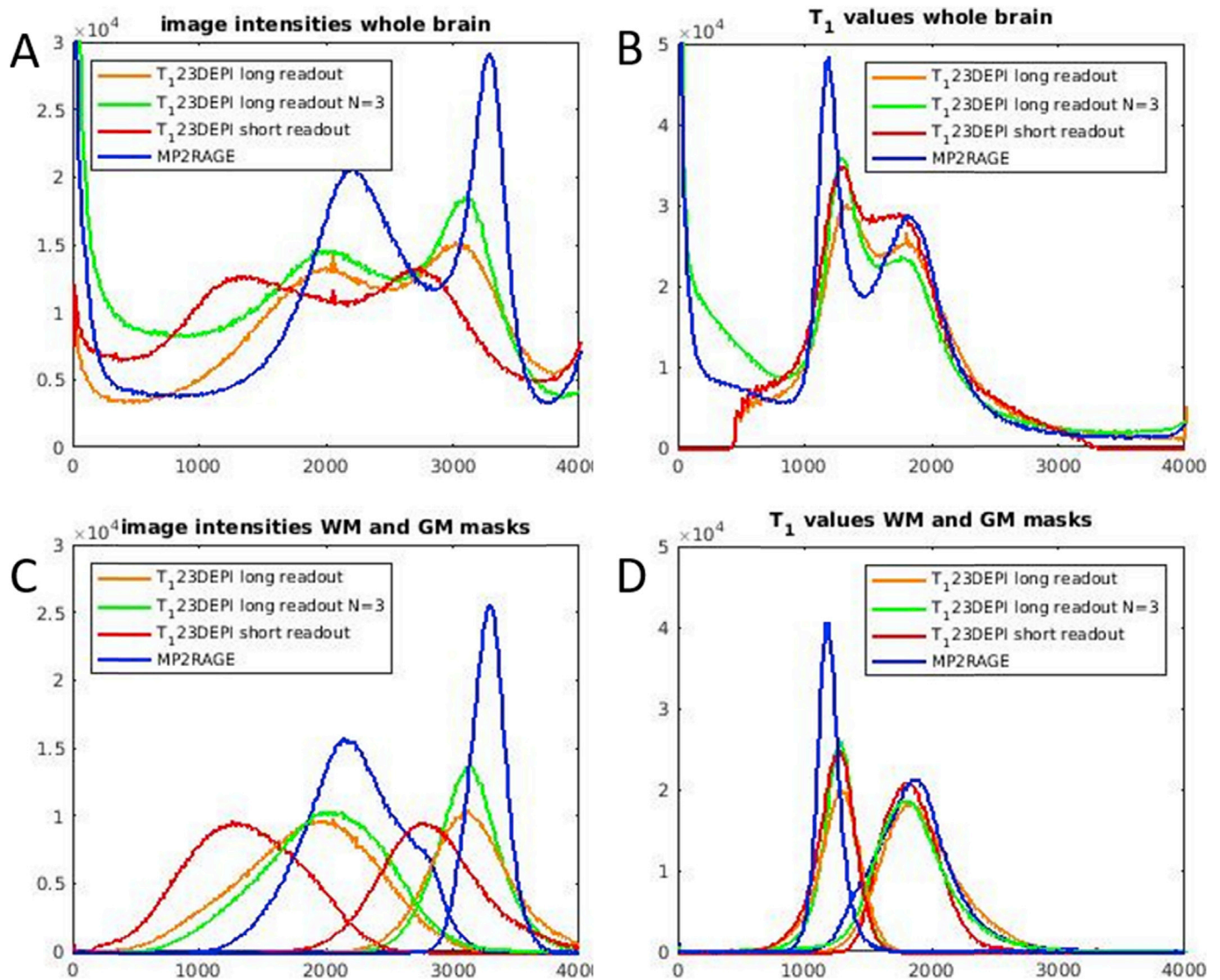


Fig. 9. Histograms for whole-brain 0.8 mm resolution data. A) Image intensities from the whole brain mask of the 0.8 mm whole-brain T₁-weighted T₁23DEPI images and MP2RAGE B) Histograms of 0.8 mm whole-brain T₁ maps and MP2RAGE T₁ maps. C) histograms of image intensities from voxels within the gray (lower values) and white (higher values) matter masks obtained from the SPM segmentation. D) histograms of T₁ values from voxels within the gray (centred around ~1800ms) and white (centred around ~1100ms) matter masks. Note that quantitative T₁ value distributions in panels b and d do not vary significantly with readout block length in the T₁23DEPI.

- For sub-millimetre protocols such as those in Experiment 1, or the 0.8 mm protocols in Experiments 2 and 3, the T₁23DEPI can be used to define the cortical surfaces needed for laminar imaging, circumventing the need for acquisition of a full anatomical scan. With the currently available software packages for cortical layer definition this approach is problematic because whole-brain coverage of the anatomy is often expected. If (semi)-manual layer definition is planned, brain coverage is less important and the T₁23DEPI data will suffice for layer definition (Fig. 5).
- A T₁23DEPI with whole-brain coverage can be segmented automatically and used for layer definition directly, completely replacing the typical anatomical acquisition. This approach has been suggested previously for other T₁-weighted acquisitions (Kashyap et al., 2017; Renvall et al., 2016). For protocols which allow the extension of the small imaging slab to cover the whole brain with equal distortions as the functional imaging, this is a very fast way of acquiring the necessary T₁-weighted data. For example, the 1 mm whole-brain dataset shown in Fig. 6 was acquired in under 3 min, the 0.8 mm whole-brain dataset in Fig. 10 in just over 3 min.

- An intermediate step between the distorted, low contrast functional data and high-contrast, non-distorted anatomical data can already greatly simplify co-registration of the two. T₁23DEPI data is high contrast and distorted, meaning co-registration between both mean EPI and the anatomy is expected to be relatively straightforward. In all protocols of both Experiment 1 and 2, the overall co-registration was successful, even for very limited slab coverage. Distortion correction schemes commonly used for the functional images, such as the TOPUP scheme applied on the data in Experiment 2c, can also be applied to the T₁23DEPIs (Fig. 7), improving the local fidelity of the anatomy-derived information. Here, we have not explored co-registration using nonlinear deformations, but the improved gray-white matter contrast should once again prove to be beneficial. Using a T₁23DEPI to aid co-registration to another anatomical scan is especially useful if the fMRI data and matching T₁23DEPI do not contain enough spatial information because of limited spatial resolution, such as for example in the case of the 1.3 mm protocol shown here (Fig. 8). Another situation, in which acquisition of a fast distortion matched T₁23DEPI will be useful, is if participants

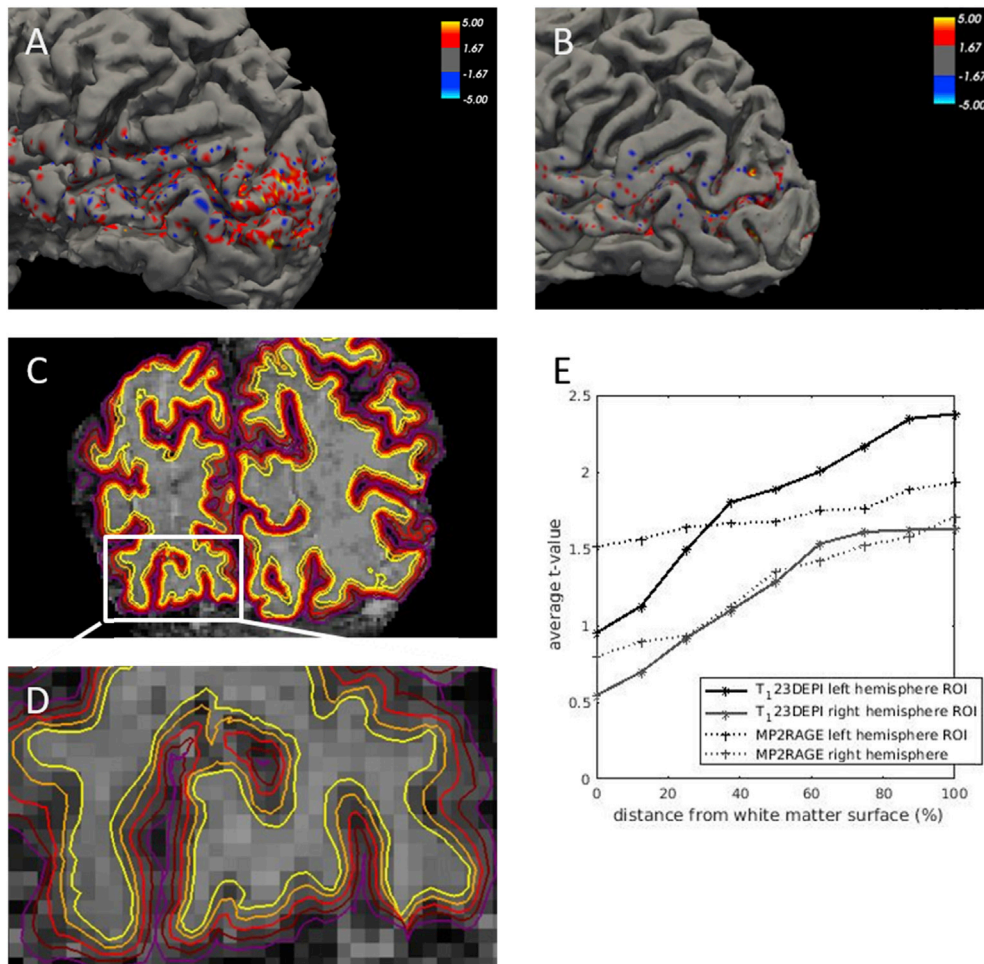


Fig. 10. Surface reconstruction and cortical depth profiles for T₁23DEPI and MP2RAGE pipelines. A) BOLD responses shown overlaid on the mid-cortical layer of the T₁23DEPI. The location of the functional imaging slab can clearly be observed. As expected, the full-field checkerboard resulted in positive BOLD responses near the occipital pole. B) BOLD responses overlaid on the mid-cortical layer of the MP2RAGE. C) Five surfaces overlaid on the T₁23DEPI and the segmentation result. Yellow: white matter surface, orange: 25%, red: 50%, wine red: 75%, purple: pial surface. The white insert indicates the region shown enlarged in panel D. E) Average t-value in left and right hemisphere ROIs as a function of cortical depth. 0% is the white matter/gray matter surface, 100% is the pial surface.

participate in multiple scanning sessions. A long anatomical acquisition will then have to be acquired only once, while the other sessions can suffice with a faster T₁23DEPI acquisition.

One of the interesting features of the current implementation of T₁23DEPI is that any fMRI acquisition protocol acquired with either a 3D or 2D EPI readout can be mimicked, even those with very long volume acquisition times. In the current implementation, the 3D-EPI volume can be separated in various blocks/segments to ensure that the optimum inversion times can be used and the amount of susceptibility-induced distortion is matched exactly to that of the fMRI images. 2D-EPI protocols can also be matched by T₁23DEPI, as distortions are predominantly present in the phase-encoding direction and the readout length of the EPI train in the T₁23DEPI can match that of most 2D-EPI protocols. Note that the assumption that distortions only occur in the phase-encoding direction breaks for 2D EPI when the bandwidth of the RF-pulses used for (simultaneous multi-) slice selection becomes comparable to the static field inhomogeneity gradients. However, even in this case the phase-encoding distortions will still be the dominant source of distortion as the EPI readout train is significantly longer than the slice selection gradient. Only 2D-EPI protocols with a very low number of slices will be difficult to match as the slab excitation profile in the T₁23DEPI will be suboptimal; requiring an extended slab in the T₁23DEPI of which the middle slices match the fMRI data, at the cost of longer scanning times for the T₁23DEPI. Even higher resolution voxel sizes than the ones presented here could also be achieved by further segmentation of the T₁23DEPI acquisitions, although the T₁-weighting also reduces SNR and hence large numbers of averages might need to be acquired. As can be seen from the 1 mm protocols for a slab and whole-

brain, the filling of the larger 3D-matrix means fewer averages need to be acquired to obtain good image SNR and white/gray matter CNR. For smaller matrices, SNR increases can be achieved through averaging of several T₁23DEPI volumes.

Comparing the T₁23DEPI to recent literature approaches mainly based on multislice imaging (Huber et al., 2016c; Kashyap et al., 2017; Renvall et al., 2016), there are two aspects that should be discussed, namely the SNR or precision of the method and the accuracy of the method. T₁-maps obtained with T₁23DEPI (based on a 2 point fit) are by definition sensitive to the validity of the single pool tissue model, which has been shown not to be fully valid 7T for white matter. On the other hand, slice selective T₁ maps are extremely sensitive to slice profile artifacts, whereby the effective flip angle varies throughout the slice. Generally, in slice-selection, flip angles will be smaller at the edges of the slice, meaning that signal locally will be less saturated by the flip angle train and a T₁-model fit which does not take this lack of saturation into account, will overestimate the T₁ value. From an SNR point of view, the T₁23DEPI SNR should be comparable or higher than what is achieved by the 2D counterparts because of the 3D nature of the acquisition and relying on two inversion times for the T₁-estimation. In Renvall et al. R₁-maps at 7T with 1 mm isotropic were obtained in 2min 56s which is on the same order of magnitude of what we have presented here (2min 30s) but no further judgements can be made on the obtained SNR. The higher number of inversion times measured by Kashyap et al. means a longer overall acquisition time, nearing 20 min (Kashyap et al., 2017). The two-shot VASO-approach using a 3D-EPI readout from Huber et al. (2016b) also lends itself to calculation of T₁-maps, though the implementation does not allow for a k-space segmentation of the 3D volume and is hence limited in the achievable spatial resolution of FOV by the

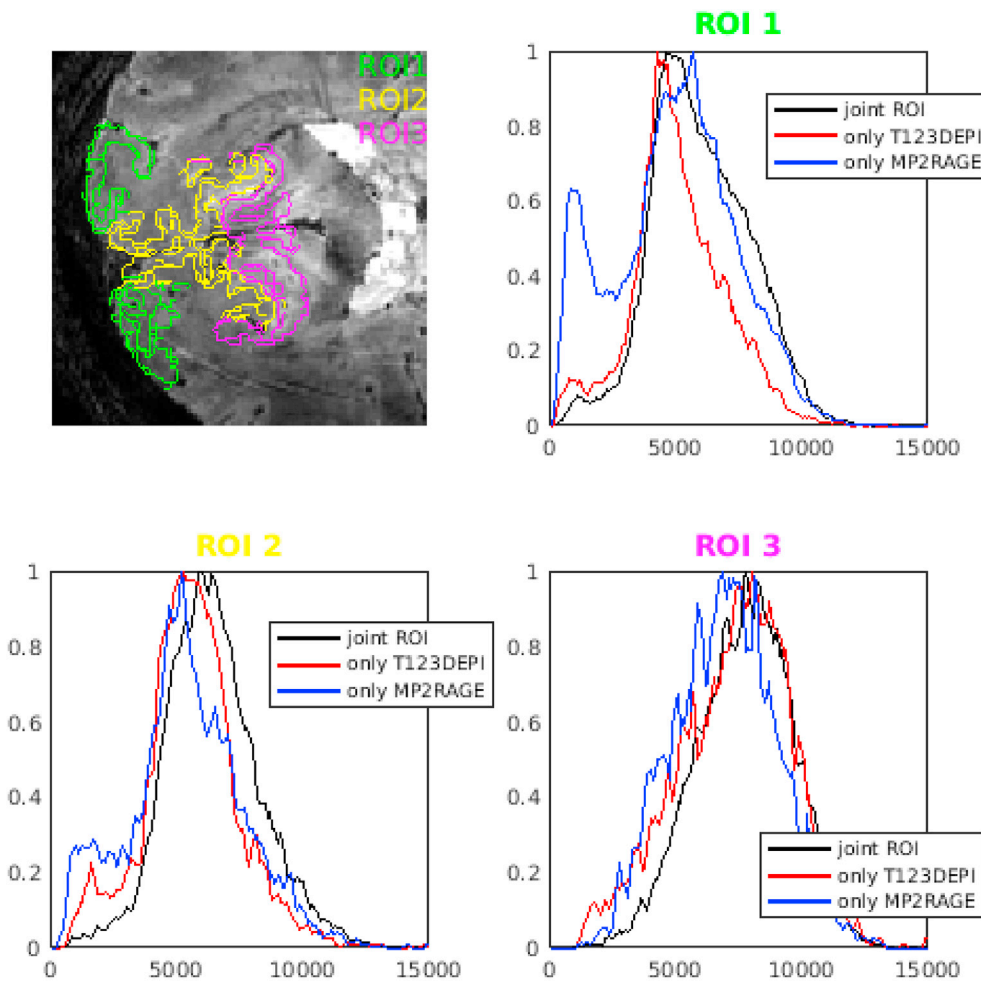


Fig. 11. Histograms of the mean EPI signal distribution in three Freesurfer-generated gray matter ROIs for the overlap between the T₁23DEPI-derived and MP2RAGE-derived segmentations. T₁23DEPI-derived ROIs are shown overlaid on the mean EPI with a continuous line and MP2RAGE-derived ROIs with a dashed line. Histograms have been normalised to facilitate the comparison between peak positions. Note that the peaks of the T₁23DEPI-only histograms are closer to the joint histogram in both ROI2 and ROI3. A shoulder of low intensity voxels is present in the histograms from ROI1 and ROI2. For the MP2RAGE-only region, this non-brain shoulder is much higher.

available gradient coil. In contrast, the current T₁23DEPI implementation allows matching of the distortions and use of ideal inversion times for any protocol because of the tailored amount of segmentation of the 3D-EPI volume.

There are disadvantages associated with the EPI readout of the T₁23DEPI also; the distortions in the T₁23DEPI T₁-weighted images make them less suitable for volumetric experiments, even if the quality is high enough for segmentation. Also, the distortions in the T₁23DEPI are assumed to be identical to those of the functional data. This requires some care that the same shim-settings are used for both acquisitions and that subjects do not move between acquisitions in such a way as to significantly change the B₀ field distribution, similar to the care taken when acquiring different runs of a functional task. The wider distribution of image intensity values in the T₁23DEPI than in the MP2RAGE (Figs. 3 and 9), in combination with the smaller difference in image intensity between the gray and white matter (Fig. 2) mean a reduced CNR compared to the longer MP2RAGE anatomical scans. The use of long readout blocks seems unadvantageous, especially if suboptimal inversion times have to be used, as the use of 4 shorter blocks rather than 2 longer ones improves the distribution of image intensities substantially (Fig. 3). In addition to the optimal inversion times, the use of shorter readouts means there is less T₁-relaxation during the readout and, hence, less T₁-induced blurring in the resulting image. The T₁-induced blurring especially affects borders between tissues of very different T₁-values, such as the gray matter/CSF border. The simulation results in Supplementary Figure 2 show that the white matter/gray matter border is not significantly affected by T₁-induced blurring for any of the simulated protocols and the gray matter/CSF border only in the 2-block protocol of

Experiment 1. Hence, not all of the difference between the histograms of the 2-block and 4-block data can be ascribed to T₁-induced blurring, a large part must be driven by the lower SNR and CNR of especially the 2-block protocol. An even larger difference in readout length was forced in Experiment 3, at 1060 ms vs 318 ms in the short block using the same flipangles in the readout train. The T₁ histograms for these data were very similar (Fig. 9), again suggesting the effect of T₁-induced blurring is limited. Nonetheless, for applications in which the point spread function is essential, such as the detection of thin structures, e.g. the Stria of Gennari or the bands of Baillarger, the T₁23DEPI point spread function can probably be improved by applying a variable-flip angle throughout the acquisition train. Such approaches have long been known for MP2RAGE (Deichmann et al., 2000).

As in the MP2RAGE sequence, the sensitivity of the specific protocol to the transmit B₁-field depends on the parameters used. The use of very long blocks (with many segments), while reducing the overall acquisition time, introduces additional transmit B₁ sensitivity because of the larger number of excitations (Marques and Gruetter, 2013). From the Bloch simulations, it is clear that the B₁ sensitivity of the 4-block T₁23DEPI protocols used in Experiment 1 was similar to that of the used MP2RAGE protocol (Supplementary Figure 1). Generally, B₁-sensitivity is lower for MP2RAGE and T₁23DEPI protocols when a smaller flip angle is used for the first GRE/EPI readout block, respectively. This, however, comes at a cost of SNR in the final image (Marques et al., 2010). A more SNR-friendly option than lowering the flip angle is the acquisition of a fast and low resolution B₁-map (Eggenchwiler et al., 2012; Nehrke et al., 2014) to correct the resulting MP2RAGE or T₁23DEPI T₁-maps (Marques and Gruetter, 2013). This is highly recommended if quantitative

T_1 -measurements are to be undertaken with the T_1 23DEPI sequence. Inversion homogeneity in the T_1 23DEPI's could be significantly improved upon by the use of a more B_1 -inhomogeneity insensitive inversion, such as the FOCI pulse. While the contrast in the presented images did not suffer noticeably from the use of the sech pulse, areas known to suffer from low B_1^+ , such as the cerebellum, would benefit from such an inversion pulse. Although the use of dielectric pads can also improve B_1 -inhomogeneity (Teeuwisse et al., 2012), the combination of pads and FOCI pulse outperforms the dielectric pads alone in such areas (O'Brien et al., 2014).

In Fig. 9 the distribution of high SNR ($N = 3$, green line) yields an only slightly narrower distribution for the T_1 23DEPI values in white matter than the equivalent 3-min scan (orange). It seems that the narrower distribution of image intensities and T_1 -values in Figs. 2 and 9 has multiple possible explanations, though even with similar T_1 -induced blurring (Fig. 9, red line); B_1^+ -inhomogeneity (Supplementary Figure 1) and SNR (Fig. 9, orange line), the difference to the MP2RAGE (Fig. 9, blue line) is not explained. This could be suggestive of an increased spread of T_1 values in the tissue/water compartment that have longer T_2^* . Note that in T_1 23DEPI the T_1 -mapping is based on signals acquired at TE 21–28ms while the MP2RAGE had a TE of 2.3ms.

For the different potential usages of this sequence mentioned above, different choices of sequence parameters might have to be made. The definition of cortical layers in a high-resolution partial brain dataset requires both high SNR and high contrast. Hence, a short block length could be used, i.e. a more aggressive segmentation of the EPI volume and/or lower excitation flip angles, to reduce T_1 -induced blurring. In addition, several averages will need to be acquired to obtain sufficient SNR. For a whole-brain acquisition, the large 3D matrix size that needs to be filled means that SNR is already high. The block length used here (~1s), comparable to standard MP2RAGE protocols, introduces some T_1 -blurring, but is nonetheless sufficiently short to yield good segmentations and surface reconstructions. Finally, if the aim is merely to aid co-registration, a faster acquisition with longer blocks and fewer averages can be considered. Note that the 2-block protocol (Fig. 3) is an example of a very fast acquisition, where the longer readouts negatively influence the image contrast (Fig. 3b) and amount of T_1 -blurring (Fig. 3d). For all protocols counts that if the user would like to obtain quantitative T_1 -values, a B_1 map based correction to remove transmit B_1 -contamination is highly recommended (Marques and Gruetter, 2013).

The SENSE artefacts in some of the fMRI data, associated with the high acceleration factors used, lead to similar artefacts in the T_1 23DEPI, locally disturbing the gray/white matter contrast. An example is indicated by the arrow in Fig. 6. The boundary of the segmentation result here presents with a less smooth surface than in neighbouring tissue. These artefacts could be avoided with the use of a more performing gradient system which would allow lower in-plane acceleration factors to be used, or the usage of k-space trajectories that exploit controlled aliasing (Bilgic et al., 2015; Narsude et al., 2015).

Nevertheless, even when using a fast, 3-min protocol, image quality in the T_1 23DEPI was sufficient to be used in a completely unmodified, automated pipeline for cortical depth dependent BOLD analysis (Fig. 10). The cortical ROI's derived from these T_1 23DEPI surfaces contained fewer non-brain voxels in the mean EPI space (Fig. 11). The benefits of an ideal co-registration outweighed here the improved SNR of the MP2RAGE.

Conclusion

Here, we introduce a sequence providing bias-field corrected T_1 -weighted images and T_1 -maps with distortions matching those of the fMRI data, ' T_1 -imaging with 2 3D-EPIs', or T_1 23DEPI. A range of T_1 23DEPI data is shown with resolutions ranging from 0.7 mm to 1.3 mm isotropic and acquisition times ranging from 80 s to 170 s. Co-registration quality to the mean EPI of matching fMRI timecourses were compared to co-registration of a standard MP2RAGE to the same volume and showed markedly less local deviations. Wholebrain T_1 23DEPI data were of

sufficient quality to be used directly for cortical surface generation, but an alternative use would be to include them in a coregistration pipeline as intermediate step.

Acknowledgements

The authors would like to thank Ritu Bhandari for sharing data and Pierre-Louis Bazin and Christian Keyzers for useful discussions. The Spinoza Centre is a joint initiative of the University of Amsterdam, Academic Medical Center, VU University, VU University Medical Center, Netherlands Institute for Neuroscience and the Royal Netherlands Academy of Sciences.

Appendix A. Supplementary data

Supplementary data related to this article can be found at <https://doi.org/10.1016/j.neuroimage.2018.04.026>

References

- Andersson, J.L.R., Skare, S., Ashburner, J., 2003. How to correct susceptibility distortions in spin-echo echo-planar images: application to diffusion tensor imaging. *NeuroImage* 20, 870–888. [https://doi.org/10.1016/S1053-8119\(03\)00336-7](https://doi.org/10.1016/S1053-8119(03)00336-7).
- Batson, M.A., Petridou, N., Klomp, D.W.J., Frens, M.A., Neggers, S.F.W., 2015. Single session imaging of cerebellum at 7 Tesla: obtaining structure and function of multiple motor subsystems in individual subjects. *PLoS One* 10, e0134933. <https://doi.org/10.1371/journal.pone.0134933>.
- Bilgic, B., Gagoski, B.A., Cauley, S.F., Fan, A.P., Polimeni, J.R., Grant, P.E., Wald, L.L., Setsompop, K., 2015. Wave-CAIPI for highly accelerated 3D imaging. *Magn. Reson. Med.* 73, 2152–2162. <https://doi.org/10.1002/mrm.25347>.
- Bodurka, J., Ye, F., Petridou, N., Murphy, K., Bandettini, P.A., 2007. Mapping the mri voxel volume in which thermal noise matches physiological noise-implications for fMRI. *NeuroImage* 34, 542–549. <https://doi.org/10.1016/j.neuroimage.2006.09.039>.
- Brammer, M.J., Bullmore, E.T., Simmons, A., Williams, S.C., Grasby, P.M., Howard, R.J., Woodruff, P.W., Rabe-Hesketh, S., 1997. Generic brain activation mapping in functional magnetic resonance imaging: a nonparametric approach. *Magn. Reson. Imaging* 15, 763–770.
- Deichmann, R., Good, C.D., Josephs, O., Ashburner, J., Turner, R., 2000. Optimization of 3-D MP-RAGE sequences for structural brain imaging. *NeuroImage* 12, 112–127. <https://doi.org/10.1006/nimg.2000.0601>.
- Dumoulin, S.O., Fracasso, A., van der Zwaag, W., Siero, J.C.W., Petridou, N., 2017. Ultra-high field MRI: advancing systems neuroscience towards mesoscopic human brain function. *NeuroImage*. <https://doi.org/10.1016/j.neuroimage.2017.01.028>.
- Eggenchwiller, F., Kober, T., Magill, A.W., Gruetter, R., Marques, J.P., 2012. SA2RAGE: a new sequence for fast B_1^+ -mapping. *Magn. Reson. Med.* 67, 1609–1619. <https://doi.org/10.1002/mrm.23145>.
- Gowland, P., Mansfield, P., 1993. Accurate measurement of T_1 in vivo in less than 3 seconds using echo-planar imaging. *Magn. Reson. Med.* 30, 351–354.
- Greve, D.N., Fischl, B., 2009. Accurate and robust brain image alignment using boundary-based registration. *NeuroImage* 48, 63–72. <https://doi.org/10.1016/j.neuroimage.2009.06.060>.
- Huber, L., Dimo, I., Marrett, S., Panwar, P., Uludağ, K., Bandettini, P.A., Poser, B.A., 2016a. Blood Volume fMRI with 3D-epi-vaso: Any Benefits over SMS-vaso. Presented at the ISMRM, Singapore.
- Huber, L., Goense, J., Kennerley, A.J., Trampel, R., Guidi, M., Reimer, E., Ivanov, D., Neef, N., Gauthier, C.J., Turner, R., Möller, H.E., 2015. Cortical lamina-dependent blood volume changes in human brain at 7 T. *NeuroImage* 107, 23–33. <https://doi.org/10.1016/j.neuroimage.2014.11.046>.
- Huber, L., Ivanov, D., Handwerker, D.A., Marrett, S., Guidi, M., Uludağ, K., Bandettini, P.A., Poser, B.A., 2016b. Techniques for blood volume fMRI with VASO: from low-resolution mapping towards sub-millimeter layer-dependent applications. *NeuroImage*. <https://doi.org/10.1016/j.neuroimage.2016.11.039>.
- Huber, L., Marrett, S., Handwerker, D.A., Thomas, Adam, Gutierrez, B., Ivanov, D., Poser, B.A., Bandettini, P.A., 2016c. Fast Dynamic Measurement of Functional T_1 and gray Matter Thickness Changes during Brain Activation at 7T. Presented at the ISMRM, Singapore.
- Hutton, C., Bork, A., Josephs, O., Deichmann, R., Ashburner, J., Turner, R., 2002. Image distortion correction in fMRI: a quantitative evaluation. *NeuroImage* 16, 217–240. <https://doi.org/10.1006/nimg.2001.1054>.
- Irfanoglu, M.O., Modi, P., Nayak, A., Hutchinson, E.B., Sarlls, J., Pierpaoli, C., 2015. DR-BUDDI (Diffeomorphic Registration for Blip-Up blip-Down Diffusion Imaging) method for correcting echo planar imaging distortions. *NeuroImage* 106, 284–299. <https://doi.org/10.1016/j.neuroimage.2014.11.042>.
- Jorge, J., Grouiller, F., Gruetter, R., van der Zwaag, W., Figueiredo, P., 2015. Towards high-quality simultaneous EEG-fMRI at 7 T: Detection and reduction of EEG artifacts due to head motion. *NeuroImage* 120, 143–153. <https://doi.org/10.1016/j.neuroimage.2015.07.020>.
- Karantanas, A.H., Papanikolaou, N., Vasiou, K., Lavdas, E., 1999. Comparison of T_1 -weighted spin-echo and 3D T_1 -weighted multi-shot echo planar pulse sequences in

- imaging the brain at 1T. *Magn. Reson. Imaging* 17, 663–668. [https://doi.org/10.1016/S0730-725X\(99\)00009-0](https://doi.org/10.1016/S0730-725X(99)00009-0).
- Kashyap, S., Ivanov, D., Havlicek, M., Poser, B.A., Uludağ, K., 2017. Impact of acquisition and analysis strategies on cortical depth-dependent fMRI. *NeuroImage*. <https://doi.org/10.1016/j.neuroimage.2017.05.022>.
- Kemper, V.G., De Martino, F., Emmerling, T.C., Yacoub, E., Goebel, R., 2017. High resolution data analysis strategies for mesoscale human functional MRI at 7 and 9.4T. *NeuroImage*. <https://doi.org/10.1016/j.neuroimage.2017.03.058>.
- Kok, P., Bains, L.J., van Mourik, T., Norris, D.G., de Lange, F.P., 2016. Selective activation of the deep layers of the human primary visual cortex by top-down feedback. *Curr. Biol.* 26, 371–376. <https://doi.org/10.1016/j.cub.2015.12.038>.
- Koopmans, P.J., Barth, M., Orzada, S., Norris, D.G., 2011. Multi-echo fMRI of the cortical laminae in humans at 7 T. *NeuroImage* 56, 1276–1285. <https://doi.org/10.1016/j.neuroimage.2011.02.042>.
- Marques, J.P., Gruetter, R., 2013. New developments and applications of the MP2RAGE sequence—focusing the contrast and high spatial resolution R1 mapping. *PLoS One* 8, e69294. <https://doi.org/10.1371/journal.pone.0069294>.
- Marques, J.P., Kober, T., Krueger, G., van der Zwaag, W., Van de Moortele, P.-F., Gruetter, R., 2010. MP2RAGE, a self bias-field corrected sequence for improved segmentation and T1-mapping at high field. *NeuroImage* 49, 1271–1281. <https://doi.org/10.1016/j.neuroimage.2009.10.002>.
- Marques, J.P., Norris, D.G., 2017. How to choose the right MR sequence for your research question at 7T and above? *NeuroImage*. <https://doi.org/10.1016/j.neuroimage.2017.04.044>.
- Mougin, O., Abdel-Fahim, R., Dineen, R., Pitiot, A., Evangelou, N., Gowland, P., 2016. Imaging gray matter with concomitant null point imaging from the phase sensitive inversion recovery sequence. *Magn. Reson. Med.* 76, 1512–1516. <https://doi.org/10.1002/mrm.26061>.
- Mugler, J.P., Brookeman, J.R., 1990. Three-dimensional magnetization-prepared rapid gradient-echo imaging (3D MP RAGE). *Magn. Reson. Med.* 15, 152–157. <https://doi.org/10.1002/mrm.1910150117>.
- Narsude, M., Gallichan, D., van der Zwaag, W., Gruetter, R., Marques, J.P., 2015. Three-dimensional echo planar imaging with controlled aliasing: a sequence for high temporal resolution functional MRI. *Magn. Reson. Med.* <https://doi.org/10.1002/mrm.25835>.
- Nehrke, K., Versluis, M.J., Webb, A., Börner, P., 2014. Volumetric B1 (+) mapping of the brain at 7T using DREAM. *Magn. Reson. Med.* 71, 246–256. <https://doi.org/10.1002/mrm.24667>.
- O'Brien, K.R., Magill, A.W., Delacoste, J., Marques, J.P., Kober, T., Fautz, H.-P., Lazeyras, F., Krueger, G., 2014. Dielectric pads and low- B1+ adiabatic pulses: complementary techniques to optimize structural T1 w whole-brain MP2RAGE scans at 7 tesla. *J. Magn. Reson. Imaging JMRI* 40, 804–812. <https://doi.org/10.1002/jmri.24435>.
- Petridou, N., Italiaander, M., van de Bank, B.L., Siero, J.C.W., Luijten, P.R., Klomp, D.W.J., 2013. Pushing the limits of high-resolution functional MRI using a simple high-density multi-element coil design. *NMR Biomed.* 26, 65–73. <https://doi.org/10.1002/nbm.2820>.
- Polimeni, J.R., Fischl, B., Greve, D.N., Wald, L.L., 2010. Laminar analysis of 7T BOLD using an imposed spatial activation pattern in human VI. *NeuroImage* 52, 1334–1346. <https://doi.org/10.1016/j.neuroimage.2010.05.005>.
- Polimeni, J.R., Renvall, V., Zaretskaya, N., Fischl, B., 2017. Analysis strategies for high-resolution UHF-fMRI data. *NeuroImage*. <https://doi.org/10.1016/j.neuroimage.2017.04.053>.
- Renvall, V., Witzel, T., Wald, L.L., Polimeni, J.R., 2016. Automatic cortical surface reconstruction of high-resolution T1 echo planar imaging data. *NeuroImage* 134, 338–354. <https://doi.org/10.1016/j.neuroimage.2016.04.004>.
- Teeuwisse, W.M., Brink, W.M., Webb, A.G., 2012. Quantitative assessment of the effects of high-permittivity pads in 7 Tesla MRI of the brain. *Magn. Reson. Med.* 67, 1285–1293. <https://doi.org/10.1002/mrm.23108>.
- Van de Moortele, P.-F., Auerbach, E.J., Olman, C., Yacoub, E., Uğurbil, K., Moeller, S., 2009. T1 weighted brain images at 7 Tesla unbiased for Proton Density, T2* contrast and RF coil receive B1 sensitivity with simultaneous vessel visualization. *NeuroImage* 46, 432–446. <https://doi.org/10.1016/j.neuroimage.2009.02.009>.
- van der Zwaag, W., Buur, P.F., Fracasso, A., van Doesum, T., Uludağ, K., Versluis, M.J., Marques, J.P., 2018. Examples of sub-millimeter, 7T, T1-weighted EPI datasets acquired with the T123DEPI sequence. *NeuroImage*. <https://doi.org/10.1016/j.neuroimage.2018.04.026>.
- van der Zwaag, W., Francis, S., Bowtell, R., 2006. Improved echo volumar imaging (EVI) for functional MRI. *Magn. Reson. Med.* 56, 1320–1327. <https://doi.org/10.1002/mrm.21080>.
- Wright, P.J., Mougin, O.E., Totman, J.J., Peters, A.M., Brookes, M.J., Coxon, R., Morris, P.E., Clemence, M., Francis, S.T., Bowtell, R.W., Gowland, P.A., 2008. Water proton T1 measurements in brain tissue at 7, 3, and 1.5 T using IR-EPI, IR-TSE, and MPRAGE: results and optimization. *Magma N. Y. N.* 21, 121–130. <https://doi.org/10.1007/s10334-008-0104-8>.
- Yacoub, E., Shmuel, A., Logothetis, N., Uğurbil, K., 2007. Robust detection of ocular dominance columns in humans using Hahn Spin Echo BOLD functional MRI at 7 Tesla. *NeuroImage* 37, 1161–1177. <https://doi.org/10.1016/j.neuroimage.2007.05.020>.
- Zimmermann, J., Goebel, R., De Martino, F., van de Moortele, P.-F., Feinberg, D., Adriany, G., Chaimow, D., Shmuel, A., Uğurbil, K., Yacoub, E., 2011. Mapping the organization of axis of motion selective features in human area MT using high-field fMRI. *PLoS One* 6, e28716. <https://doi.org/10.1371/journal.pone.0028716>.